Numerical Investigation of Breaking Waves Impact On a Vertical Wall With a Large Recurved Parapet

Yasmine Ben Belkacem, Gaële Perret, Julie Lebunetel, Grégory Pinon

Proceedings of the Thirty-third (2023) International Ocean and Polar Engineering Conference **www.isope.org**
Ottawa, Canada, June 19-23, 2023

ISBN 978-1-880653-80-7; ISSN 1098-6189

Numerical Investigation of Breaking Waves Impact On a Vertical Wall With a Large Recurved Parapet

Yasmine BEN BELKACEM[1,2]*, Gaële PERRET*[1]*, Julie LEBUNETEL*[2] *and Grégory PINON*[1]

[1] Laboratoire Ondes et Milieux Complexes, UMR 6294 CNRS, Normandie Univ, UNIVLEHAVRE, Le Havre, France.
[2] INGÉROP Conseil et Ingénierie, Rennes , France.

ABSTRACT

The present work describes the numerical approach used for the assessment of breaking waves impact on a vertical wall with a large recurved parapet , for which experiments were performed in Coastal Research Centre (ForschungsZentrum Küste, FZK), Hannover, Germany (Ravindar et al., 2018, 2019, 2021).
To perform these computations, the compressible multi-phase solver within the OpenFOAM numerical toolbox is presently combined with the waves2FOAM libraries to generate waves and resolve the Navier Stokes equations. Moreover, in these considered solvers, the free surface is treated using the Volume of Fluid (VoF) method and the pressure-velocity equations are solved thanks to the PIMPLE algorithm.
Different wave gauges and pressure probes are present in the experimental configuration that are used either as input parameters for our simulations and for the validation of our numerical results by numerical-experimental cross-comparisons.

KEY WORDS: OpenFOAM; relaxation zones; breaking waves; impact pressure; compressibility effects.

INTRODUCTION

Coastal structures are built to prevent land erosion and flooding. They can appear in different shapes, among which vertical breakwaters and sea walls are frequently used. However, these structures can be severely damaged when subjected to violent sea state conditions. Oumeraci et *al.* (1993) reported that breaking waves are the most significant cause of this damage but, on the other hand, they state that the prediction of design wave load conditions remains difficult. This means that accurate investigation of waves loading is a key factor for a safe design of coastal infrastructures.
Extreme wave loadings have been underlined both theoretically (e.g. Cooker & Peregrine, 1990) and experimentally (e.g. Kirgkoz 1982; Oumeraci et *al*. 1993; Hattori et *al*., 1994 and Bullock et *al*., 2007). Most of these studies gave a general classification of breaking wave loads on vertical and sloping sea walls. Besides, it has been proven that the shape of breakwaters has a large influence on the so-called wave impact pressure exerted on the structure, and the wave over-topping as well (Hull and Müller, 2002). In fact, nowadays, with the sea level rise due to global warming, rather than increasing the sea wall height, many researchers and engineers show that adding a parapet could be more efficient in mitigating the wave over-topping through discharging a part of seawater back into the sea.

Some early physical and empirical studies were carried-out by Owen & Steel (1992), Cornett et *al.* (1999) and Kortenhaus et *al.* (2001, 2003) to investigate the efficiency of different types of parapets (plain or recurved). Recently, more laboratery-based research work has been made in this context (e.g. Ravindar et *al.*, 2019, 2021; Ravindar & Sriram 2021; Stagonas et *al.*, 2020) focusing on the forces and the impact pressure at the structures with a recurved retrofitting.
Stagonas et *al.* (2020) and Ravindar et *al.* (2020, 2021) have performed two sets of experiments on the vertical wall attached with recurved parapets. The model scale (1:8) experiments conducted in a shallow wave flume at the Department of Ocean Engineering, Indian Institute of Technology (IIT) in India, and the quasi-prototype scale (1:1) carried out at Large Wave Flume (Großer Wellen Kanal, G.W.K.) in Hanover, Germany. Different parapets (with different angles of extension) and wave conditions were tested, and all experiments consider a single monochromatic wave field, which will lead to breaking owing to the presence of a sloping beach in front of the vertical wall. The small-scale (1:8) configuration was scaled using the Froude scaling method which unfortunately creates scale effects due to its limitations. For this reason, the large-scale experiments (1:1) with, to the author point of view, more reliable results avoiding scale effects will be preferred for the purpose of this paper.

The experimental facilities are usually expensive and limited, as a result, a detailed parametric study is not always feasible. However, with the significant advances of High-Performance Computing, several parametric simulations could be carried out and validated with experiments, using different Computational Fluid Dynamics (CFD) tools. Particularly, the open-source library OpenFOAM based on the Finite Volume Method (FVM) and using the Volume of Fluid (VoF) approach has been applied to investigate various problems related to coastal and offshore engineering. The good capabilities of this software were demonstrated by Morgan et *al.*, (2010), Liu et *al.*, (2019) and more recently by Molines et *al.*, (2020) who numerically modelled

the wave hydrodynamics on rubble mound breakwaters with different geometries of parapets using OpenFOAM and validated with model scale experiments. Although, many research works have been published in numerical modeling of wave-structure interactions, the literature about waves impact on recurved parapets in breaking wave conditions is still very limited and remains a challenging task.

In the present work, the multi-phase compressible solver interFOAM is combined with the waves2FOAM toolbox (Jacobsen et *al.*, 2012), to simulate waves propagation and impact on a vertical wall equipped with a large recurved parapet. More precisely, the aim of this study is to reproduce numerically the free surface behaviour and impact pressures of breaking waves on a large-scale structure, for which experiments were performed by Stagonas et *al.* (2014), Ravindar et *al.* (2020) and Ravindar and Sriram (2021). Our numerical results are later compared with the experimental measurements and some previous studies already focusing on this configuration (Benoit et *al.*, (2022), Li et *al.*, (2022), Zheng et *al.*, (2022)).

NUMERICAL MODELLING

Governing equations

An Euler-Euler approach within the *compressible* solver is used to carry out this study, where the air phase is compressible and assumed to be a perfect gas, while water is modelled as a weakly compressible liquid. *Compressible* interFOAM generally solves the three-dimensional unsteady Navier-Stokes equations for an homogeneous and immiscible two-phase fluid. Here, only a 2D configuration will be considered: use of 3D solver with a single mesh cell in one direction.
The general Navier-Stokes equations governing both phases are written as a mass conservation equation (eq .1) and a momentum balance equation (eq .2) listed as follows:

$$\frac{\partial \rho}{\partial t} + \nabla \cdot (\rho \mathbf{u}) = 0, \tag{1}$$

$$\rho\left(\frac{\partial \boldsymbol{u}}{\partial t} + \boldsymbol{u} \cdot \nabla \boldsymbol{u}\right) = -\nabla p + \nabla \cdot \left[\mu\left(\nabla \boldsymbol{u} + (\nabla \boldsymbol{u})^T - \frac{2}{3}(\nabla \cdot \boldsymbol{u})\underline{\boldsymbol{I}}\right)\right] + \boldsymbol{S}, \tag{2}$$

where ρ is the fluid density, $\boldsymbol{u}$ is the velocity vector field, p is the fluid pressure, μ is the dynamic viscosity, $\underline{\boldsymbol{I}}$ is the identity tensor and $\boldsymbol{S}$ stands for the external body representing here the gravity term $\rho \boldsymbol{g}$. Here, bold terms represent vectors.

These governing equations are discretized into a finite number of cells and time steps. The space discretization is performed by the finite volume method (FVM) based on unstructured meshes with arbitrary continuous polyhedral cells that form a control volume. The aforementioned differential equations are afterwards linearized, integrated and interpolated over each control volume using the Gauss scheme. In addition, the equations are discretized in time using the bounded-implicit Euler scheme. The coupled pressure-velocity equation is solved using the PIMPLE algorithm, which combines the PISO (Pressure Implicit with Splitting Operators) (Issa, 1985) and SIMPLE (Semi Implicit Method for Pressure Linked Equations) (Ferziger and Peric, 1999) methods. A self-adjusted time step Δt and controlled by a given maximum Courant Number Co (Courant et *al*, 1967) is applied in order to ensure the stability and the accuracy of the numerical model. The Courant number is defined as:

$$Co = \frac{\Delta t}{\Delta x}|u|, \tag{3}$$

where Δt is the maximum time step, Δx is the cell size in the main velocity direction and $|u|$ is the velocity magnitude.

Free surface treatment

In the present numerical work, the Volume of Fluid (VoF) technique is employed to track the phase interface. This method is presented by Hirt and Nichols (1981) and is based on the volume fraction concept. The two-phase fluid is considered as an Eulerian mixture and each of the phases has a separately defined volume fraction denoted $\alpha(x, t)$ and ranging between zero and the unity as follows:

$$\alpha(x,t) = \begin{cases} 0, & \text{air} \\ 1, & \text{water} \\ 0 < \alpha < 1, & \text{interface} \end{cases} \tag{4}$$

The density and dynamic viscosity could therefore be expressed as of function of α:

$$\begin{aligned} \rho &= \alpha \rho_{water} + (1-\alpha)\rho_{air} \\ \mu &= \alpha \mu_{water} + (1-\alpha)\mu_{air} \end{aligned} \tag{5}$$

To determine the volume fraction α, an advection equation should be solved:

$$\frac{\partial \alpha}{\partial t} + \nabla \cdot (\alpha \boldsymbol{u}) + \nabla \cdot (\alpha(1-\alpha)\boldsymbol{u_r}) = 0, \tag{6}$$

where the last term of the left-hand side of equation 6 represents an artificial compression. It is to ensure the non-smearing of the free surface and limit the numerical diffusion. $\boldsymbol{u_r}$ is defined as the relative compression velocity. In the considered solver, the interface capturing is performed using the Gauss MUSCL scheme and the MULES algorithm (Multidimensional Universal Limiter with Explicit Solution).

Waves modelling

The Waves2Foam libraries developed by Jacobsen et *al*., (2012) are used to generate and absorb different incident waves. For this purpose, the Waves2Foam employs the relaxation zone (RZs) method which acts like an active sponge layer. More precisely, the relaxation zones are added into the numerical domain to gradually blend between a target ϕ_{target} and a computed $\phi_{computed}$ solution depending on the selected wave theory (in the inlet relaxation zone), and force them to match at the boundary. The blending function reads:

$$\phi(x,t) = \gamma_R(x)\phi_{computed}(x,t) + (1-\gamma_r(x))\phi_{target}(x), \tag{7}$$

where ϕ is either the velocity field $\boldsymbol{u}$ or the volume fraction α, and γ_R is the relaxation function or the weight field (Fuhrman et *al.*, 2006), which is defined as:

$$\gamma_R(\chi_R) = 1 - \frac{e^{\chi_R^{3.5}} - 1}{e - 1} \leftarrow \chi_R \in [0:1]. \tag{8}$$

This blending procedure is applied at each time step on the velocity and VoF fields.

VALIDATION AND NUMERICAL SETUP

The forthcoming section is divided into two sub-sections. The first subsection will focus on validating our numerical model by analyzing the waves propagation phase only, whereas the second one will present the 2D numerical setup for modelling the breaking waves on the GWK large-scale configuration (Stagonas et *al.*, 2020). Both configurations consider the same Stokes second-order waves with a period of $T = 6$ s, a wave height of H= 0.7 m and a wave length of $\lambda = 35.13$ m in the deeper part of the wave flume.

Grid convergence analysis for waves propagation without sloping beach and curtained wall

A validation study is initially carried out to assess the capabilities of the numerical model to accurately generate and propagate regular waves. For this purpose, a simple rectangular numerical wave tank (NWT) in 2D is considered (see Fig. 1). The total length of the computational domain is L_x = 243 m, exactly the same length as the GWK configuration. Stokes second-order waves are generated at a water depth of h = 4.1 m using relaxation zones method. Two relaxation zones are defined at the inlet (wave generation) and the outlet (wave energy dissipation) of the NWT, and have lengths of $L_{RZi} = 2\lambda$ and $L_{RZo} = 3\lambda$ respectively, allowing a proper generation and absorption of the incident waves.

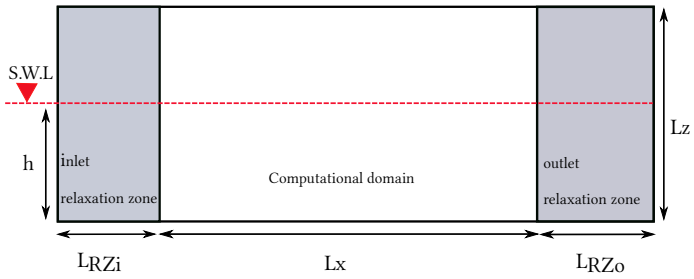

Fig. 1 : 2D Numerical wave tank dimensions.

So far boundary conditions are concerned, no-slip conditions are applied to the bottom of the NWT; atmospheric pressure conditions are assigned to the top boundary defined as an open boundary, where water and air can freely flow out. The inlet and outlet boundaries have the velocity and free surface conditions prescribed by the relaxation zone method. A structured grid is used over the computational domain and four sets of meshes dh of 1 m, 0.5 m , 0.25 m, and 0.1 m are tested to perform the convergence analysis (see Table 1). The computational mesh is further refined around the free surface leading to a cell aspect ratio of $\Delta x/\Delta z = 5$, where Δx is the cell resolution in the horizontal direction and Δz refers to the cell height. The time discretization is controlled by a maximum Courant number condition of maxCo=0.4 in the whole computational domain. Finally, the total physical time duration is defined as $20T$ to be fully converged and the computations are processed using 12 cores.

Table 1 : Grid convergence mesh parameters and RMSE values.

Mesh size	***dh* = 1 m**	***dh* = 0.5 m**	***dh* = 0.25 m**	***dh* = 0.1 m**
Total number of cells [-]	5016	20925	83700	514632
Number of cells per wavelength [-]	35	70	141	351
Computational cost [min.]	2.1	4.7	20.7	488.6
RMSE [m]	0.027	0.030	0.026	0.024

Numerical free surface elevation profiles obtained at $t = 80\,s$ as a function of the NWT length are compared to the analytical waveform of Stokes second-order in Fig. 2. As shown, the present numerical computations well converge to the desired analytical profile from a grid size of $dh = 0.5\,m$, while a coarser mesh of $dh = 1\,m$ under-predicts the wave height due to larger numerical diffusion. Furthermore, a root mean square error (RMSE) is evaluated using equation 9:

$$RMSE = \sqrt{\frac{1}{N}\sum_{i=1}^{N}(\eta_i - \eta_{Ni})^2}, \tag{9}$$

where η_i represent analytical free surface elevations and η_{Ni} the corresponding numerical ones.

As one can read, the RMSE values presented in Table 1 are very low and reveal that the used numerical model accurately reproduce second-order Stokes theory. Although this could seem easy and straightforward, it was not so because the chosen parameters indicate that the current wave is in fact in the range of second-order Stokes theory but in its upper limit and close to the third order. Of course, the quality of the wave propagation is even better with finer grid size. As computation of impact is challenging, the smaller $dh = 0.1\,m$ is finally chosen for the subsequent simulations.

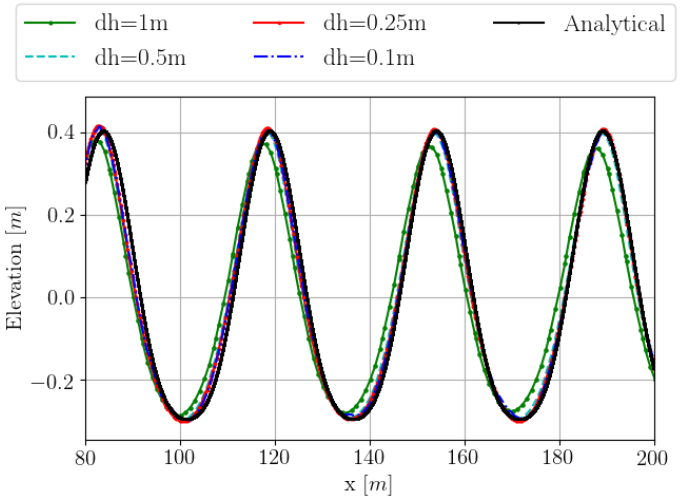

Fig. 2 : Spatial convergence study based on free surface elevations.

Numerical setup for impinging waves on the GWK configuration

Experimental setup

The large-scale experiments (Stagonas et *al.*, 2014, 2020) are carried-out in the Große WellenKanal (GWK, Hannover, Germany). This large wave flume is 307 m long, 5 m width and 7 m depth. Incident waves are being generated using a piston-type wave-maker controlled hydraulically and equipped with an active wave absorption system. In the considered experiments, a coastal structure consisting of a vertical wall and a recurved parapet is installed at the end of a 1/10 sloping beach covering a distance of 33 m as illustrated in Fig. 3. The geometry and dimensions of the parapet are shown in Fig. 3b. In order to evaluate the impact of breaking waves on this structure, twelve wave gauges are fixed along the wave flume with distances from the wave generation zone varying from 50 m (WG 1) to 235 m (WG 12). In addition, sixteen pressure probes (PP1 to PP16, Fig.1b) with a high acquisition frequency of f_s = 5000 Hz are distributed along the vertical wall and the parapet to record pressure signals. The set of these different probes will be further used in the numerical-experimental cross-comparison. More details about the experimental tests can be found in Stagonas et *al.*, (2020) and Ravindar et *al.*, (2020, 2021).

Numerical mesh and computational parameters

The numerical wave tank is represented from the wave-maker to the structure location giving a computational domain of 243 m long. Regarding the height of the NWT, the top boundary is taken higher than the top of the parapet to prevent any numerical issues related to air velocities with the water impact. One inlet relaxation zone of two waves

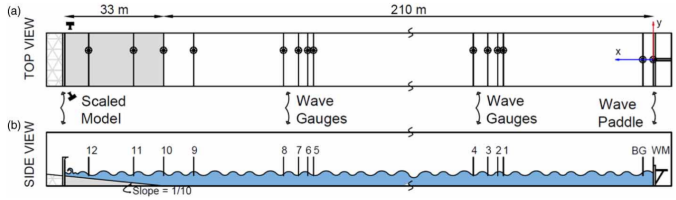

(3a)

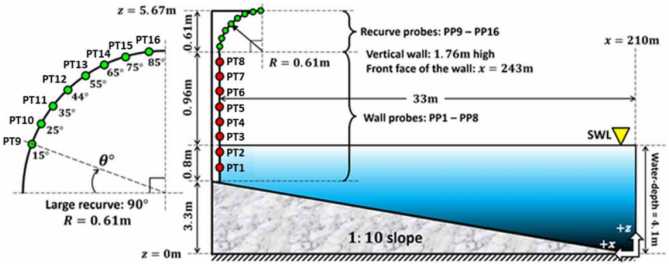

(3b)

Fig. 3 : Sketch of the experimental setup in 1:1 scale. (3a) Top and side view of the wave flume with the wave gauges; (3b) sketch of the vertical wall with recurved parapet and the pressure transducers locations. Reprinted from Ravindar et *al.*, 2022.

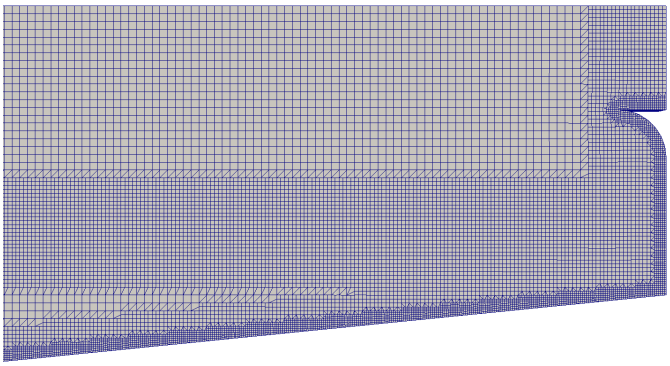

Fig. 4 : Numerical mesh snapshot in the vicinity of the sloping beach and the structure.

length ($L_{RZi} = 2\lambda$) is defined to generate and propagate the aforementioned regular waves and absorb the reflected ones. The mesh consists of hexahedral and split-hex cells and being built as follows (see Fig. 4):

- a first level of refinement where both cell characteristic sizes are divided by 2 is applied around the free surface area (defined from $-H$ below and $+H$ above the SWL); 1 m before the structure (wall and the top part of the parapet) and along the sloping beach,
- a second level of refinement where both cell characteristic sizes are further divided by 2 is also applied in the close proximity of the structure and the sloping beach.

The mesh is finally composed of 565,365 cells.

NUMERICAL RESULTS AND DISCUSSION

In this section, free surface elevations, impact pressure on the structure and total impact force are presented, analysed and compared to the experimental measurements provided by Ravindar and Sriram (2021, unpublished notes) in the case of waves impact with a small air pocket. The presently used configuration was the one identified at the ISOPE 2022 Benchmark "Comparative study on Breaking Waves Interactions with Vertical Wall Attached with Recurved Parapet in Small and Large scale "already studied by other teams and published along with the ISOPE 2022 conference by Benoit et *al.*, (2022), Li et *al.*, (2022), Zheng et *al.*, (2022).

Since a compressible solver is being used, both phases satisfy now an equation of state (EoS) of perfect fluids and their thermo-physical properties are initially defined and set to a pressure of 1 bar and a temperature of 293 K. In fact, the compressible formulation is more adapted for studying wave slamming on a wall due to its ability to capture the compressibility of the fluids and attempt to model the pressure peaks more accurately when compared to the incompressible formulation. This was demonstrated in Batlle Martin et *al.*, (2021) where a good convergence of the pressure impulse is obtained under the incompressible assumption but the maximum pressure peaks never converge and keep increasing with the mesh refinement. Other studies of the same research team were performed on a similar topic highlighting the importance of using a compressible solver Lu et *al.*, (2021) and Batlle Martin et *al.*, (2023).

Besides, an adaptive time-step is applied for the time discretisation using a maximum Courant Number of $maxCo = 0.4$, the latter is later reduced to $maxCo = 0.15$ in an attempt to capture possible impulsive loads. Depending on the studied case, turbulence is either neglected or modelled by the *standard* $k - \omega$ SST turbulence model.

Unless mentioned, the following computations are processed using 140 cores of Intel Broadwell (2.4 GHz) in CRIANN (Centre Régional Informatique et d'Applications Numériques de Normandie) to compute 178 events, exactly the same value as in the experiments. The computational cost of each case is outlined in Table. 2.

Table 2 : Computational cost of the GWk configuration using a mesh of 565,365 cells.

Case	***CFL = 0.4***	***CFL = 0.4 + k-ω SST***	***CFL = 0.15***
Nb of cores	140	140	140
Computational cost [hours]	≈ 15	≈ 9	≈ 35

Free surface elevation

Fig. 5 presents free surfaces evolution over time recorded by 4 numerical wave gauges. The presented results are shifted in time so that the maximum elevation happens at the same instant for all the data (*i.e* a $\Delta t_{Num} = 0.7s$ for both $maxCo = 0.4$ and $maxCo = 0.15$). In general, obtained numerical profiles compare very well with the experimental ones. WG1 and WG5 are used to assess the quality of wave generation; the simulated signals at these waves gauges exhibit very good agreement, confirming the ability of the numerical model to accurately propagate waves.

WG10 is used to check if any reflection appears at this transition between the flat bottom and the beginning of the sloping beach. Both numerical and experimental results show to have the same shape and height for the main waves crests and troughs. However, some minor discrepancies can be noticed on the secondary peak: in fact, at this location, waves start breaking resulting in a highly distorted free surface with complex shapes. Finally, WG12 located just in front of the recurved parapet, is employed to analyse reflection properties due to impinging wave on the structures. Satisfactory agreement is also demonstrated suggesting that the present numerical model is able to accurately reproduce wave generation and propagation, together with possible wave reflection on the structure.

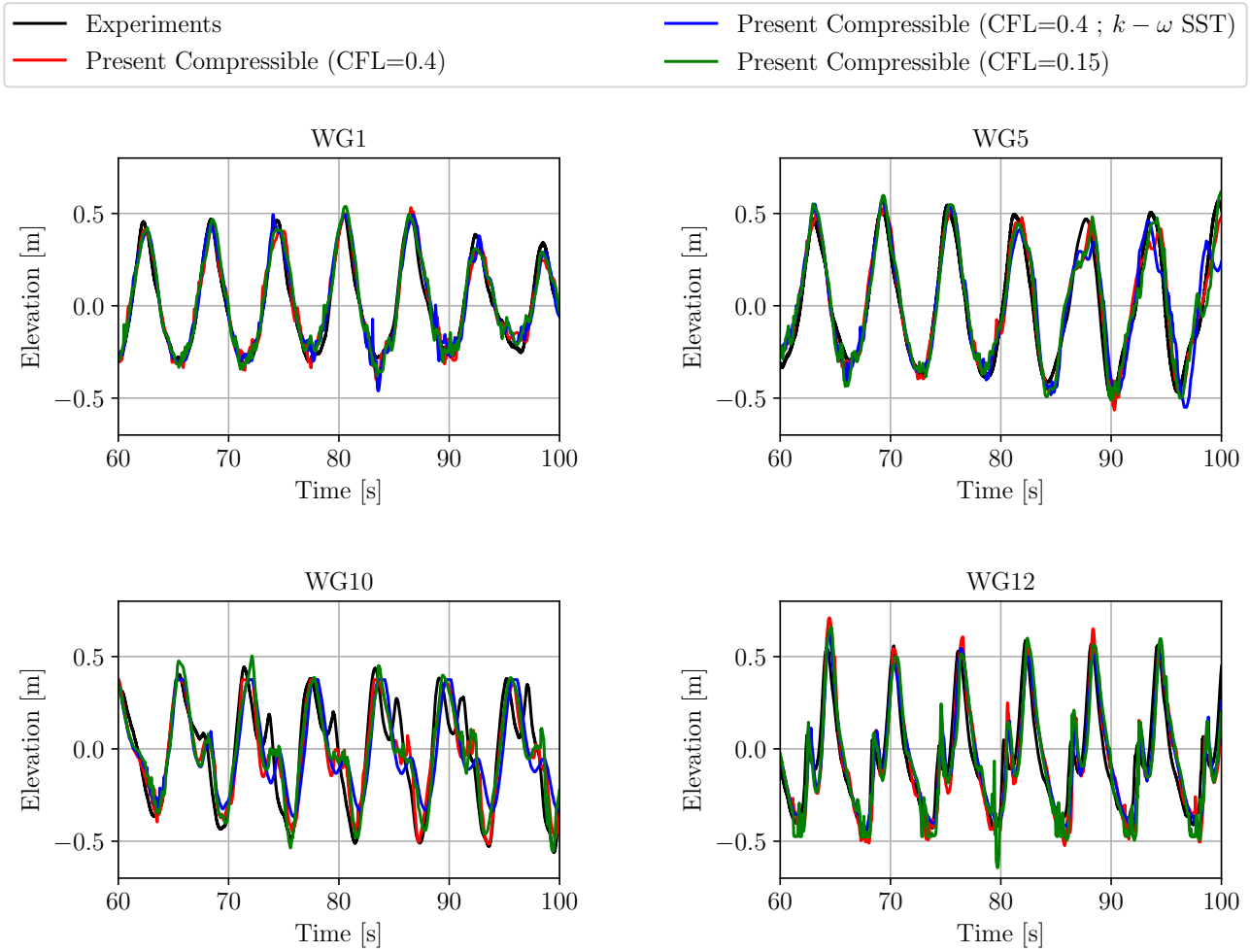

Fig. 5 : Experimental and numerical comparison of free surface elevation time series at wave gauges WG1, WG5, WG10 and WG12

For the gauge close to the structure, no real decay can be identified both numerically and experimentally indicating that the physics seems to be accurately reproduced.

Impact pressure

Fig. 7 depicts temporal series of pressure at four out of the sixteen pressure probes. The overall numerical results are found to be matching well with the experiments; the general trend of the pressure distribution is indeed properly captured by the present numerical model as illustrated in Fig. 6.

In fact, both numerically and experimentally, a sharp and very high pressure peak is recorded indicating an impulsive impact followed by a pressure dome of much lower magnitude. A very small phase delay may be noticeable from time to time between the different impact pressures, but nothing important. As expected, impact pressure maxima on the structure occurs at probes PP1, PP2 (below SWL) and PP3 (above SWL), which is consistent with the observations reported by Bullock et *al.*, (2007). From the zoom-in window presented at the top-left corner of Fig. 6, pressure oscillation are well noticeable in the experimental measurements (black line) most probably indicating the important role of an air pocket while the wave is breaking. Also, occurrence of sub-atmospheric pressure right after the peak, which is a common feature due to the decompression of the entrapped air pocket (Oumeraci et *al.*, 1993) is also observable.

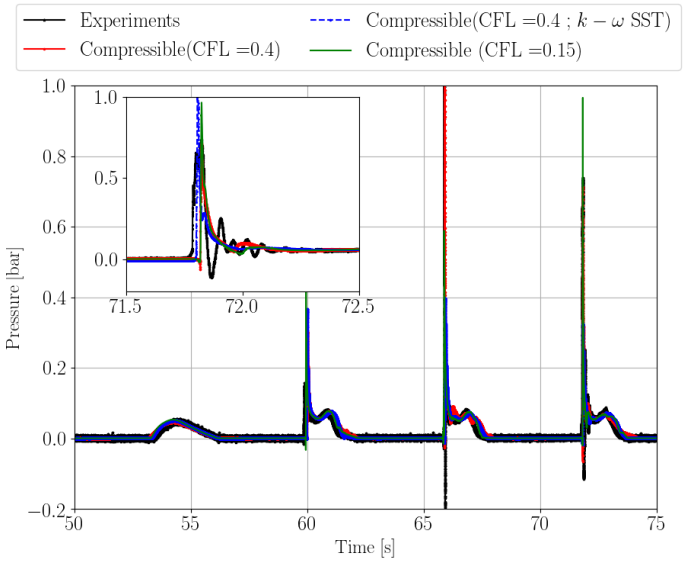

Fig. 6 : Numerical and experimental pressure signals at PP3 and a zoom on a single event around t = 72 s.

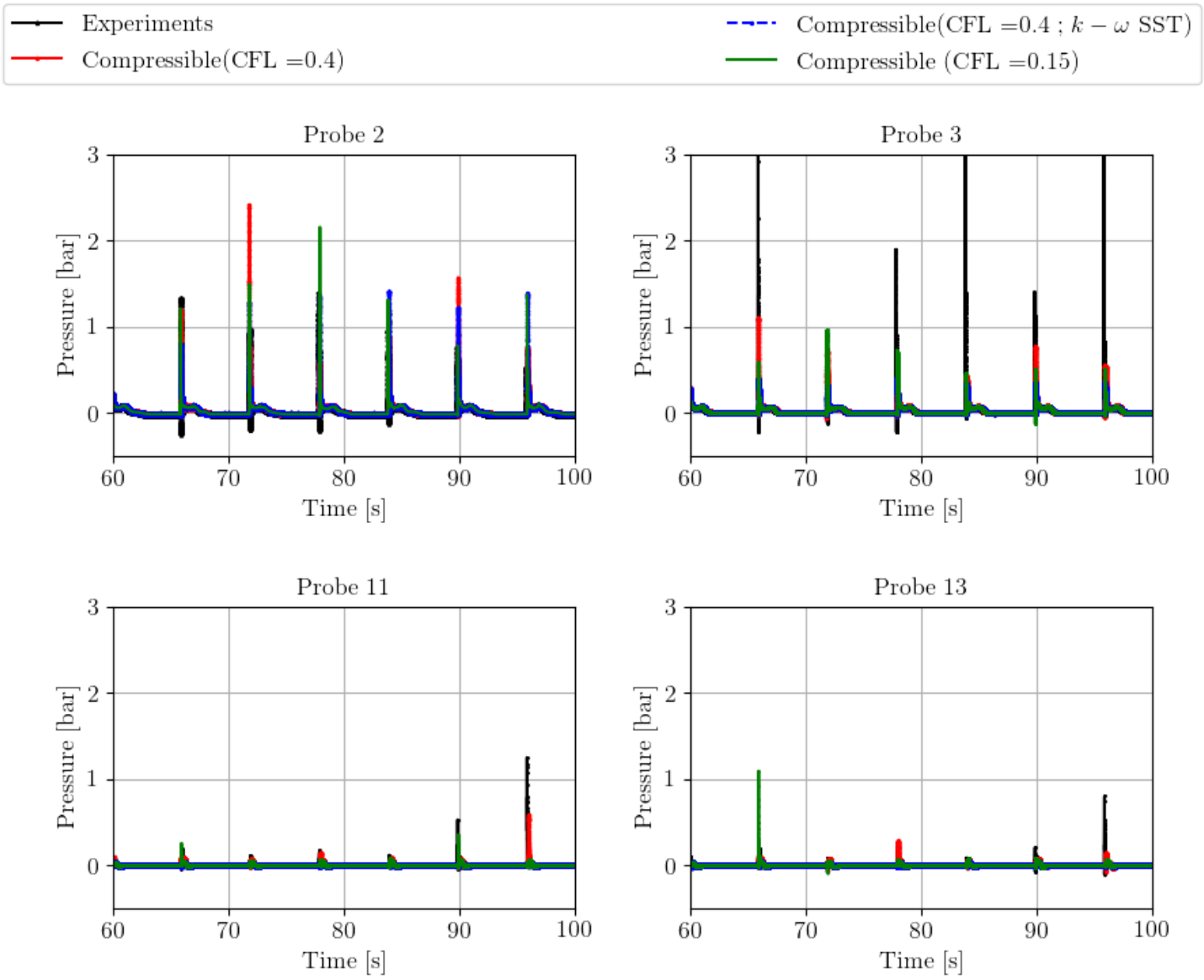

Fig. 7 : Experimental and numerical comparison of pressure impact time series at several probe locations.

Unfortunately, these are not captured by the present numerical model, both with $maxCo = 0.4$ and $maxCo = 0.15$ with the finest mesh discretisation of $dh = 0.1\,m$. These differences are most probably due to still a too low mesh resolution around the vertical wall. In fact, in some previous studies, either on this case by (Benoit et *al.*, 2022) or in the case of solitary wave impact by (Batlle Martin et *al.*, 2021), such oscillations were numerically obtained but with even increased temporal and spatial discretizations. This will consists of one of the direction to consider in the following. An important feature of coastal protection studies is how to accurately assess impulsive loads. In fact, from Fig. 7 (probes 2 and 3) and Fig. 6, it could be observed that the maximum impulsive pressure is not always exactly reproduced, most of the time the experimental one being above as depicted in Fig. 7 (probe 3). In order to better assess the statistical representativeness of such results, the averaged value of the pressure maxima for each impact was evaluated and presented in Fig. 8. In other words, an average over the 178 peak pressures values was calculated and presented in Fig. 8.

From the presented results, it was found that the current numerical model largely underestimates the maximum values of the impulsive pressure at probes lying close to the free surface (PP2, PP3, PP4, PP5) mostly. Refining the time-step, by decreasing the maximum Courant number from 0.4 to 0.15, slightly improves the results. But this is absolutely not sufficient at the current stage. Moreover, and possibly as one could expect, these results showed that no improvement was obtained with the addition of the turbulence model.

As a matter of partial conclusion, the numerical behaviour may be further improved by reducing, as much as possible, the spatial and temporal resolution. This may lead to even more computationally demanding simulations. But this will be the aim of the following of this work. Answering the questions: is such a numerical CFD approach able to replicate the experimental extrema? And, if yes, quantifying the numerical resource necessary to do so in real size configuration, which is nearly the case with this present experimental configuration at (GWK), is clearly the scope of the ongoing work. A closer look at the 3D effects might also

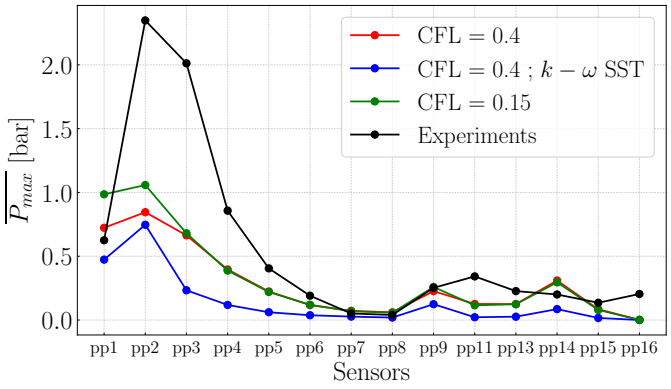

Fig. 8 : Averaged value of the pressure maximum (peak pressure) at all the probes locations.

be worthwhile.

Finally, regarding the sensors located on the recurved parapet (e.g. PP11 and PP13), both experiments and numerical data showed to be of the same magnitude. In fact, when the wave collapses on the vertical wall, it looses a large part of its energy during the impact before reaching the parapet. However, in the framework of global warming, bearing in main that dike will need to be refurbished possibly with the addition of parapet on the existing structure, assessing the load on the parapet is worthwhile. For such study cases, the present numerical configuration seems to answer the question and reveals to be sufficient already.

Impact force

Fig. 9 depicts the total force exerted on the structure, aligned with the wave propagation direction. The total impact force is evaluated by an integration method following Ravindar et *al.*, (2022) and reads:

$$F_{tot}(t) = \frac{1}{2}\sum_{i=1}^{N}\left[\left(p_i(t) + p_{i+1}(t)\right)\cdot \Delta z_i\right], \tag{10}$$

where $p_i(t)$ is the calculated instantaneous pressure at the i^{th} pressure probe, Δz_i is the distance between two consecutive probes and N stands for the total number of the pressure transducers, which is 16.

One can easily recognize the impact peaks and the negative force induced by the sub-atmospheric pressures (see. Fig. 9), which are the most relevant features of the impact with an air pocket. A qualitative analysis of the force signals is carried out and presented in Fig. 10 by using numerical snapshots of three relevant instants during a wave impact. The different images show the dynamics and kinematics of the flow before impact t_b, during $t_{impact} = t_i$ and after impact t_1. In the first image, corresponding to an instant just before impact, the wave front is overturning while approaching to the structure and entrapping an air pocket. The rise time is evaluated to 18.4 ms and, during this period, the pressure induced force is largely increased from the configuration where only the bottom part of the wall is in contact with the water (see Fig 10a and b for $t_b = 65.78\ s$) and all the wall is undergoing a large impact pressure (see Fig 10a and b for $t_{impact} = 65.92\ s$). During the initial impact stages, the wave energy is lost resulting in a deceleration of the flow and a transfer of momentum upwards creating a water jet which rises and curls over the recurved parapet (see the last flow and velocity field snapshots in Fig. 10c).

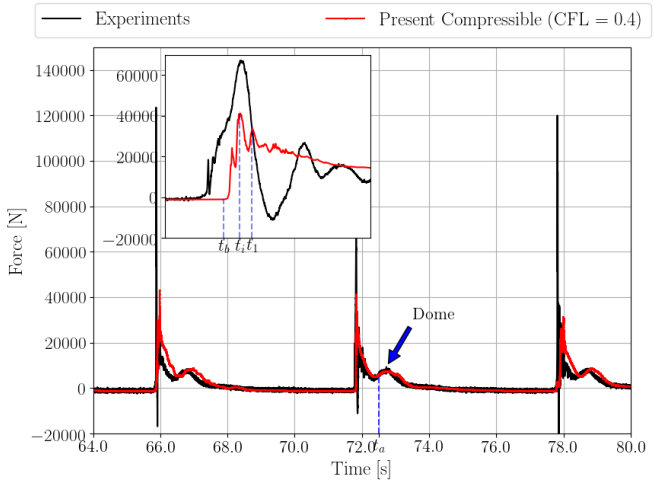

Fig. 9 : Numerical time history of the wave impact induced forces on the structure obtained with eq. 10.

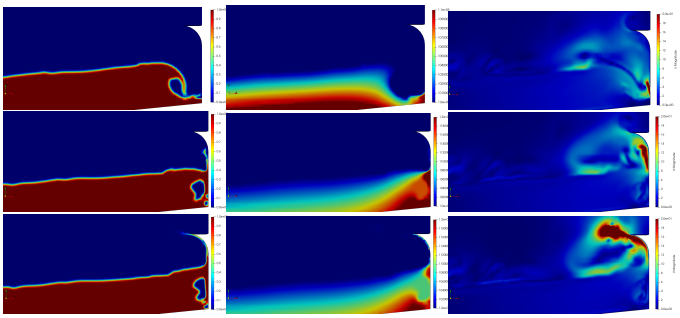

(10a) (10b) (10c)

Fig. 10 : Snapshots of (a) water volume fraction, (b) pressure P (Pa) and (c) velocity magnitude U (m/s) during the rise time $t_b = 65.78\ s$, at the impact $t_{impact} = 65.92\ s$ and after at $t_1 = 65.98\ s$.

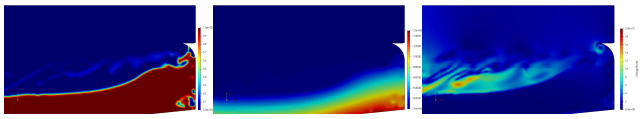

(11a) (11b) (11c)

Fig. 11 : Snapshots of (a) water volume fraction, (b) pressure P (Pa) and (c) velocity magnitude U (m/s) after the impact, presented by the blue arrow in Fig 9.

After the main peak in the force time series, due to very large impulsive pressures (see Fig 6), a dome in the force time series is always encountered. This dome is in fact noticeable at $t \approx 67\ s$, $t \approx 73\ s$ and $\approx 79\ s$ from Fig. 9. Fig. 11 depicts snapshots of the water volume fraction, velocity and pressure fields after the impact, indicated by a blue arrow in Fig. 9 at approximately $t_a \approx 72.6\ s$. These snapshots may explain the presence of this dome in the force, most probably due to dynamic pressure of the bulk water of the wave (Fig. 11a). This feature in the force time series is due to the energy conversion of the horizontal wave velocity in dynamic pressure (a dome is also observable in Fig. 6) and hence into an horizontal force.

CONCLUSION

The presented study focused on numerical simulations of breaking wave impacts on a vertical wall equipped with a large recurved parapet. The used configuration and experimental data are provided in the framework of the ISOPE-2022 benchmark. Here, the quasi-prototype scale (1:1) experiments carried out in the Large Wave Flume (GroßerWellen Kanal, G.W.K.) in Hannover (Germany) were considered and numerically reproduced. Following the configuration tested in the ISOPE-2022 benchmark, only a single monochromatic second-order Stokes wave is tested, close to the third-order theory.

In that respect, an Eulerian two-phase compressible model within the OpenFOAM toolbox has been chosen to perform the computations. The choice of a compressible solver was motivated by a previous study in our research group where solitary wave impact on a vertical wall were tested (Batlle Martin *et al.*, (2021) and Lu *et al.*, (2021)), also highlighting some very impulsive impact configurations but also on some other more applied configurations such as in Batlle Martin *et al.*, (2023). For the current configuration, the relaxation zone method was also used for the wave generation as in the previous study. Here, the numerical model was first validated on wave generation and propagation by comparing numerical results with analytical free surface elevations, for instance. A mesh independence study was also carried out highlighting a nice convergence of the results.

As impact configurations are concerned, the finest mesh discretisation was finally chosen together with two CFL conditions ($maxCo = 0.4$ and $maxCo = 0.15$). Activation of a turbulence model (k-ω SST) was also activated for a configuration to assess its role in the obtained results. The full 243 m-long flume tank of GWK was modelled in the computations and very accurate results were obtained on the free surface elevations considering comparison with the experimental wave gauges; either placed just after the wave generation or near to the wall. From this point of view, the computation are fully validated. Seconds, the impact pressures time series are compared with the 16 experimental pressure probes that are located all over the wall up to the upper part of the recurved parapet. In that respect, shape of the pressure series are well reproduced numerically, showing a succession of impacts starting with a very high pressure peak followed by a secondary dome and then a flat pressure record until the next impact. However, some discrepancies are now observed: maximum values of the pressure peaks are largely underestimated numerically and pressure oscillations following the first impulsive impact are not very accurately reproduced. The smaller CFL condition ($maxCo = 0.15$) slightly improve both of these observed discrepancies but still not accurately replicates experimental results. On the contrary, the use of a turbulence closure, here the k-ω SST model, accentuate these discrepencies.

In the last part of the paper, snapshots of water volume fraction, velocity and pressure fields were used to analysed these results also looking at integral forces acting on the structure. This last aspect of force evaluation on the whole structure and also on the recurved parapet are for some industrial perspectives when actual dikes will need to be retrofitted due to sea level rise, possibly with the addition of a recurved parapet.

As a continuation of the study, possible even finer discretisations, both spatially and temporarilly, may be considered to assess possible improvements in comparisons with the experimental results. Also, an estimation of the numerical cost of such simulations will be performed to better estimate if using Computational Fluid Dynamics is affordable in dike and parapet design phase? And if not, how far are we from this being achievable?

ACKNOWLEDGEMENTS

The authors would like to acknowledge Dr. V. Sriram and Er. R. Ravindar (IIT Madras, India), Dr. D. Stagonas (Univesity of Cyprus, Cyprus) and Dr. Z.Xie (Cardiff Universiry., United Kingdom) , for sharing all the experimental data from the aforementioned GWK configuration.

YBB also acknowledges Ingerop for the funding of her PhD grant. GPe and GPi acknowledge the financial support of the Agence Nationale de la Recherche , through the program Investissements d'avenir - LabEx EMC3 via the project PERCUSS. The present work was performed on computing resources provided by CRIANN (Normandy, France).

REFERENCES

Batlle Martin, M., Pinon, G., Reveillon, J., Kimmoun, O., (2021). "Computations of soliton impact onto a vertical wall: Comparing incompressible and compressible assumption with experimental validation ", *Coastal Engineering*, Vol 164, 103817. https://doi.org/10.1016/j.coastaleng.2020.103817

Batlle Martin, M., Pinon, G., Barajas, G., Lara, J.L., Reveillon, J. (2023). "Computations of pressure loads on an oscillating water column with experimental comparison for random waves ", *Coastal Engineering*, Vol 179, 104228. https://doi.org/10.1016/j.coastaleng.2022.104228

Benoit, M., Benguigui, W., Teles, M., Robaux, F., Peyrard, C. (2022). "Two-phase CFD simulation of breaking waves impacting a coastal vertical wall with a recurved parapet ", *Proceedings of the* 32nd *International Ocean and Polar Engineering Conference*. ISBN 978-1-880653-81-4; ISSN 1098-6189.

Bullock, G., Obhrai, C., Peregrine, D., Bredmose, H., (2007). "Violent breaking wave impacts. Part 1: Results from large-scale regular wave tests on vertical and sloping walls ", *Coastal Engineering*, Vol 54, pp 602–617.

Cooker, M., Peregrine, D. (1992). "Wave impact pressure and its effect upon bodies lying on the sea bed ", *Coastal Engineering*, Vol 18, pp 205-229.

Cornett, A., Tarbotton, M., Mattila, M., Gittens, G. (1999). "Model study of wave loads on a new cruise ship pier for Bridgetown, Barbados ", *Proc. of the Canadian Coastal Conference*.

Courant, R., Friedrichs, K., Lewy, H. (1967). "On the partial difference equations of mathematical physics ", *IBM J. Res.Dev*, Vol 11- Issue 2, pp 215–234..

Ferziger, J.H., Peric, M. (1999), "Computational methods for fluid dynamics ", *Second ed. Springer*, Berlin, 440.

Hattori, M., Arami, A., Yui, T. (1994). "Wave impact pressure on vertical walls under breaking waves of various types", *Coastal Engineering*, Vol 22, pp 79-114..

Hirt, C.W., Nichols, B.D. (1981), "Volume of fluid (VOF) method for the dynamics of free boundaries ", *Journal of computational physics*, Vol 39, 201-225.

Hull, P., Müller, G. (2002). "An investigation of breaker heights, shapes and pressures ", *Ocean Engineering*, 29 (1), 59–79.

Jacobsen, N.G., Fuhrman, D.R., Fredsøe, J. (2012). "A wave generation toolbox for the opensource CFD library: OpenFoam ", *International Journal for Numerical Methods in Fluid*, 70(9): 1073–1088.

Kirkgoz, M.S. (1982). "Shock pressure of breaking waves on vertical walls ", *Journal of Waterway, Port, Coastal and Ocean Division*, 108, 81–95

Kortenhaus, A., Pearson, J., Bruce, T., Allsop, N., Van der Meer, J. W. (2003), "Influence of parapets and recurves on wave overtopping and wave loading of complex vertical walls ", *Coastal Structures*, 369–381.

Li, Q., Yan, S., Ma, Q., Zhang, N. (2022). "Numerical investigation of breaking wave interaction with vertical wall attached with recurved parapet using qaleFOAM ", *Proceedings of the* 32nd *International Ocean and Polar Engineering Conference*. ISBN 978-1-880653-81-4; ISSN 1098-6189.

Liu, S., Gatin, I., Obhrai, C., Ong, M. C., Jasak, H. (2019). "CFD simulations of violent breaking wave impacts on a vertical wall using a two-phase compressible solver ", *Coastal Engineering 154*, 103564.

Lu, X., Cherfils, J-M., Pinon, G., Rivoalen, E., Kimmoun, O., Brossard, J. (2021). "SPH numerical computations of wave impact onto a vertical wall with experimental comparisons ", *Comptes Rendus. Mécanique*, Tome 349, 1. https://doi.org/10.5802/crmeca.72

Molines, J., Bayón, A., Gómez-Martín, M. E., Medina, J. R. (2020). "Numerical study of wave forces on crown walls of mound breakwaters with parapets ", *Journal of Marine Science and Engineering 8 (4)*, 276.

Morgan, G., Zang, J., Greaves, D., Heath, A., Whitlow, C., Young, J., (2010). "Using the rasInterFoam CFD model for wave transformation and coastal modelling ", *Proceedings of 32nd Conference on Coastal Engineering*. Shanghai, China, 2010.

Oumeraci H. (1994). "Review and analysis of vertical breakwater failures—lessons learned ", *Coastal engineering*, 22, 3–29.

Owen, M.W., Steele, A.A.J. (1991). "Effectiveness of recurved wave return walls ", *Report SR 261, HR Wallingford*, Wallingford, UK.

Ravindar, R., Sriram, V., Schimmels, S., Stagonas, D. (2018). "Comparative study of breaking wave forces on a quasi-prototype recurved seawall ". *In Proceedings of the 4th International Conference in Ocean Engineering (ICOE 2018)*, Vol2, February, 18–21, Chennai, pp.489–501. ISBN 978-981-13-3134-3.

Ravindar, R., Sriram, V., Schimmels, S., Stagonas, D. (2019). "Characterisation of breaking wave impact on vertical wall with recurve ". *ISH Journal of Hydraulic Engineering 25*, 2. https://doi.org/10.1080/09715010.2017.1391132.

Ravindar, R., Sriram, V., Schimmels, S., Stagonas, D. (2021). "Approaches in scaling small scale experiments on the interactions of breaking waves with a vertical wall and a recurved parapet ", *Journal of Waterway, Port, Coastal and Ocean Engineering 147 (6)*, 04021034. doi:10.1061/(ASCE)WW.1943-5460.0000674.

Ravindar, R., Sriram, S. (2021). "Impact pressure and forces on vertical wall with different types of parapet ", *Journal of Waterway, Port, Coastal and Ocean Engineering 147 (3)*, 04021034. DOI:10.1061/(ASCE)WW.1943-5460.0000635.

Stagonas, D., Lara, JL., Losada, IJ., Higuera, P., Jaime, FF., Muller, G., (2014). "Large scale measurements of wave loads and mapping of impact pressure distribution at the underside of wave recurves ", *Proc HYDRALAB IV Joint User Meeting*, Lisbon, Portugal, 2-4 July, 2014.

Stagonas, D., Ravindar, R., Sriram, V., Schimmels, S. (2020). "Experimental evidence of the influence of recurves on wave loads at vertical seawalls ", *Water 12 (3)*, 889. doi:10.3390/w12030889.

Zheng, K. and Zhao, X. (2022). "Breaking waves interactions with vertical seawall attached with recurved parapet using the three-dimensional parallel CIP-based mode ", *Proceedings of the* 32nd *International Ocean and Polar Engineering Conference*. ISBN 978-1-880653-81-4; ISSN 1098-6189.